Soliton Generation and Rogue-Wave-Like Behavior Through Fourth-Order Scalar Modulation Instability

Kamal Hammani, Christophe Finot, Bertrand Kibler, Guy Millot

Soliton generation and rogue wave like behavior through fourth-order scalar modulation instability

Kamal Hammani (*IEEE Student Member*), Christophe Finot (*IEEE Member*),[*]
Bertrand Kibler and Guy Millot
Institut Carnot de Bourgogne, UMR 5209 CNRS/Université de Bourgogne, 21078 Dijon, France
[*]*Corresponding author: christophe.finot@u-bourgogne.fr*

Abstract: We numerically study the underlying nonlinear dynamics of ultra-broadband optical wavelength converters based on fourth-order scalar modulation instability. Specifically, we demonstrate the spontaneous emergence of solitons and trapped radiation waves during the frequency conversion process leading to significant blue and red spectral expansions. Furthermore, we provide a statistical analysis of both Stokes and anti-Stokes bands, showing their intensity histogram evolution as a function of the propagation towards the L-shape signature typical of rogue events.

Index Terms: Four wave mixing, Fiber nonlinear optics, Solitons

1. Introduction

Optical fiber systems are well-known to provide convenient platforms with which to investigate a large and diverse set of fascinating fundamental nonlinear phenomena [1]. Among the striking consequences of the interplay of dispersive and Kerr effects is the modulation instability (MI) [2], entailing the exponential growth of a weak perturbation at the expense of a continuous or quasi-continuous pump wave. The amplified perturbation can be either quantum noise (i.e., spontaneous MI) or a frequency shifted signal wave (i.e., induced MI). In the frequency domain, MI is equivalent to a four-photon parametric mixing process where two pump photons are annihilated to create a Stokes (signal) – anti-Stokes (idler) photon pair.

MI is often associated with the anomalous dispersion regime where it has been intensively studied, especially in the context of practical applications to optical telecommunications. MI can indeed be used for broadband optical amplifiers or for optical wavelength converters [3, 4]. However, MI is not restricted to the anomalous regime and the phase-matching condition required for the development of MI can also be fulfilled in a wide range of other experimental configurations, for example in polarization maintaining fibers [5], in bimodal fibers [6] or in normally dispersive fibers with an adequate fourth-order dispersion [7, 8]. This later configuration combined with the use of photonic crystal fibers (PCF) [9] has stimulated great attention, especially in view of the significant frequency shifts that can be achieved in wavelength conversion processes [8, 10-12]. Potential applications based on silicon nanowaveguides have also been more recently reported [13].

In this letter, we focus our attention on the spectro-temporal nature of both converted signal and idler. In particular, we report the spontaneous emergence of solitonic structures in the Stokes wave. Those solitons are then affected by the intrapulse Raman response of the fiber and further shift towards higher wavelengths. Regarding the anti-Stokes wave, we also outline that an efficient optical trapping of dispersive waves mediated by solitons leads to spectral broadening towards shorter wavelengths. Furthermore, a statistical analysis of the peak-powers of both resulting signal and idler pulses highlights a ‘rogue-wave’ like behavior with pulses deviating strongly from the average behavior.

This article is thus organized as follows. We first describe the experimental configuration we numerically model. We then detail the spectro-temporal evolution of the Stokes and anti-Stokes signals. Finally, the statistical nature of the wavelength-converted waves is investigated.

2. Context, model and parameters used

In 2003, Harvey and coworkers have reported a new modulation instability window by pumping a photonic crystal fiber in the normal dispersion regime [8]. Taking into account the dispersion up to the fourth-order, the phase matching condition can be simply written as:

$$\beta_2 \ \Omega^2 \ + \ \frac{\beta_4 \ \Omega^4}{12} + 2\,\gamma\,P = 0 \qquad (1)$$

where β_2 and β_4 represent the second and fourth-order dispersion terms respectively, γ is the nonlinear Kerr coefficient and Ω is the spectral-shift between signal or idler wave and the pump wave which has an initial peak power P. With $\beta_2 > 0$ (normal dispersion regime), this condition requires $\beta_4 < 0$. If satisfied, two narrow sidebands will emerge far from the pump.

Based on the fiber parameters provided in [8], Fig. 1(a) illustrates the phase-matching conditions and enables to predict directly the wavelengths of the Stokes and anti-Stokes waves. Therefore, it is possible to convert a visible red pump (with a central wavelength of 647 nm) into blue and near-infrared light (505 nm and 900 nm respectively). Experimental spectra recorded by Harvey *et al.* after propagation on the slow axis of a 1-m long PCF [8] are recalled in Fig. 1(b). The two narrow sidebands observed at the expected wavelengths are a clear signature of MI induced by fourth-order dispersion. It definitely confirms the potential applications of this physical process as well as the benefits of PCF that combine an enhanced Kerr non-linearity with a tailored dispersion profile. Note that recent works have demonstrated that with a careful design of the PCF structure it is possible to optimize the pump and Stokes/anti-Stokes wavelengths [10].

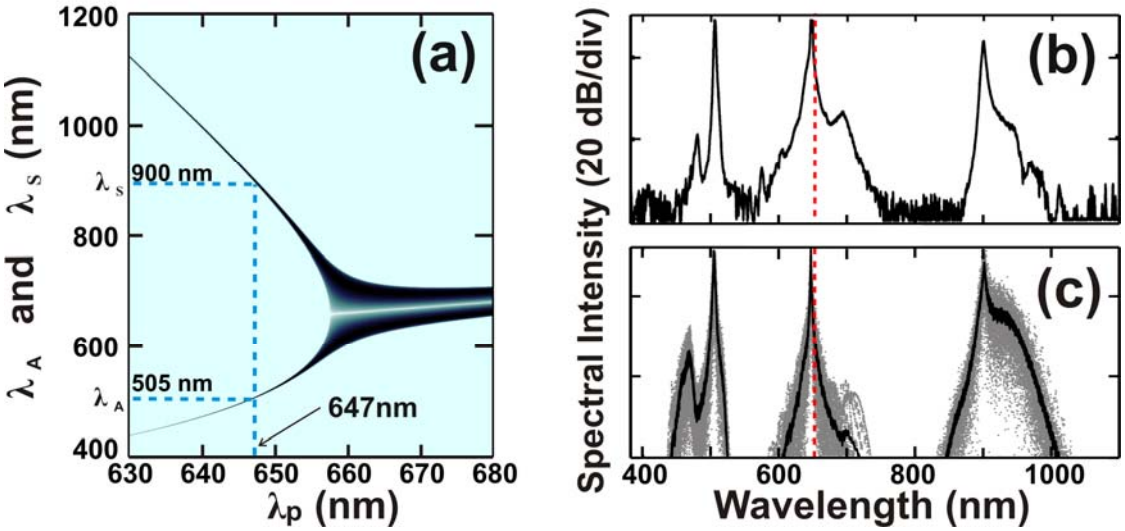

Fig. 1. **(a)** Phase-matching diagram for the fiber under investigation. The spectrum recorded **(b)** experimentally by Harvey et al. [8] is compared with our numerical results **(c)** after 1 m of propagation. We have averaged (solid black line) our results over a set of 50 "shots" (grey dotted lines). The red dashed line stands for the zero dispersion wavelength of the fiber.

The Stokes and anti-Stokes wavelengths experimentally recorded were in excellent agreement with Eq. (1). However, if we look in more details into the experimental spectrum, we can notice that the resulting MI bands are much broader that what could be expected from the stringent phase-matching conditions. More precisely, we can make out a small spectral peak located at the lower wavelength of the anti-Stokes pump as well as a significant broadening towards longer wavelengths of the Stokes. The physical origin of these spectral features has not been to our knowledge fully elucidated and several elements could provide a potential explanation. Indeed, one may suppose that the spectral expansion of the Stokes and anti-Stokes waves is somewhere related to longitudinal fluctuations in the core diameter or in the hole size [9]. It is indeed known that the resulting dispersion fluctuations are very harmful to the

appearance of modulation instabilities and can affect significantly the gain and bandwidth of the fiber component [7, 14-16]. Other potential explanations lie in the finite temporal width of the pumping that is not purely monochromatic, or in the consequences of the Raman response of silica.

In order to provide a clear explanation, we numerically investigate the evolution of the optical wave in the fiber. The longitudinal evolution of envelope *A*(z,T) of the electrical field is accurately modeled by the generalized nonlinear Schrödinger equation (GNLSE) [17, 18] :

$$\frac{\partial A}{\partial z}+\frac{\alpha}{2}A-\sum_{k=2}^{k=4}\frac{i^{k+1}}{k!}\beta_k\frac{\partial^k A}{\partial T^k}=i\gamma\left(1+i\tau_{shock}\frac{\partial}{\partial T}\right)A(z,T)\int_{-\infty}^{+\infty}R(T')\times\left|A(z,T-T')\right|^2 dT' \qquad (2)$$

with α the linear losses, β_i the i-th order dispersion coefficient, γ the nonlinear coefficient, $R(T)$ the nonlinear response of silica including both the instantaneous Kerr response and the Raman delayed contribution. The optical self-steepening is also included through τ_{shock}. The studied fiber has the following dispersive properties (for slow axis and at the pump wavelength): β_2=2.50 $ps^2.km^{-1}$, β_4=-4.49 × 10^{-5} $ps^4.km^{-1}$ for an estimated nonlinearity of 160 $W^{-1}.km^{-1}$. The initial pulse corresponds to the experimental conditions, i.e. a 70-ps pulse having a peak power of 160 W. Noise is included in the frequency domain through a one photon per mode background. Further details of the numerical model can be found in [17].

Our numerical results plotted in Fig. 1(c) are in clear agreement with the experimental results and reproduce the above mentioned spectral broadening of the Stokes and anti-Stokes waves. Note that from shot to shot, the output spectrum exhibit significant changes. That is why we have averaged our results over a set of 50 “shots” in order to get something comparable to the experimental measurement which is physically averaged. We will further detail this aspect in section 4 of the paper.

From these numerical simulations, the first conclusion we can draw is that longitudinal fluctuations are not involved in the development and location of the spectral substructures. Short-scale fluctuations can however explain the slight discrepancy observed in the level of the substructures between experimental and numerical results [15]. From complementary simulations based on a continuous wave, we have also carefully checked that, for the length of fiber under investigation, the finite picosecond duration of the pump pulse does not play a major role in the spectral evolution.

3. Spectro-temporal evolution

Now that the direct comparison with previously published experimental results has enabled us to confirm the validity of our modeling, we can gain important insights on the spectro-temporal dynamics undergone in the fiber device. We have plotted in Fig. 2(a) the spectral evolution as a function of propagation distance. Between 25 and 50 cm, the main feature is the growth of the two narrow sidebands typical of MI in the normal dispersion regime. After 50 cm of propagation, both spectral sidebands begin to continuously expand. From a practical point of view in the context of wavelength conversion, this means that the length of the fiber is a crucial parameter that should be chosen with care [10, 19].

For comparison, the longitudinal evolution recorded for a pumping in the anomalous dispersive regime with an identical absolute value of dispersion is plotted in Fig. 2(b). It is clearly apparent that the usual well-documented scalar modulation instability leads to sidebands that are much broader and closer to the pump. The resulting spectrum is also more compact. This then further confirms that the normal pumping scheme is a promising candidate for the generation of ultra-broadband supercontinua as several experimental works have recently reported [12, 19-21].

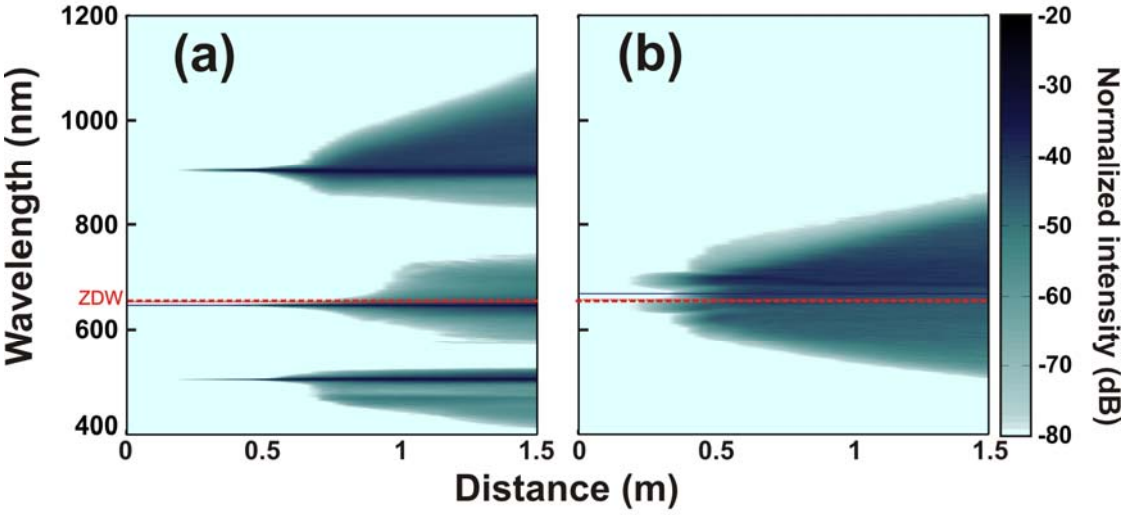

Fig. 2. Longitudinal evolution of output spectra for the propagation in a 1.5 m PCF : comparison between pumping in the normal dispersive regime **(a)** and pumping in the anomalous dispersive regime **(b)**. The red line corresponds to the ZDW. The spectra are averaged over 50 shots.

In order to clarify the physical origin of the spectral expansion observed in normally dispersive fibers, we have computed the spectrogram of a unique shot at different propagation distances (Fig. 3). This kind of representation allows a convenient derivation of both temporal and frequency evolutions from the same data. The initial long-pulse (Fig. 3(a)) is Fourier limited. At 50 cm (Fig. 3(b)), the two narrow Stokes and anti-Stokes sidebands correspond temporally to a strong modulation at the pulse center (top). This modulation breaks the quasi-continuous pump to obtain fundamental solitons (Fig. 3(c)) in the Stokes band which lies in the anomalous dispersion regime. These optical structures are ultrashort (temporal duration below 100 fs), which explains the broadening of the spectral Stokes band. In other words, the Stokes wave is far from being a coherent narrow linewidth signal and in the temporal domain, the peak power of the femtosecond solitons largely exceeds the peak power of the initial pump pulse. Let us remark that at this stage, the pump begins to be highly depleted so that the Stokes wave enters in a passive evolution not affected by MI amplification gain.

Once the broadband soliton formed and the pump depleted, the intrapulse Raman response is responsible for the progressive frequency shift (Fig. 3(d)) towards higher wavelengths (Raman soliton self-frequency shift effect [22]). This was intuitively anticipated by Kudlinski et al. in [20]. Let us however stress that we have numerically found that cross-phase modulation (XPM) in this multi-wavelength system was an additional key process taking part in the spectral expansion [12, 23, 24]. Regarding the evolution towards lower wavelengths of the anti-Stokes band, it is related to the phenomenon known as the radiation trapping by a soliton [25, 26]. This causes the spectral broadening towards lower wavelengths linked to the continuous soliton shift towards higher wavelengths. Such a behavior has been identified as a promising candidate for continuous wave supercontinua towards visible wavelengths [27, 28]. This is better illustrated in Fig. 4(a) which is a magnification of Fig. 3(d). An optical structure located at T = 43.3 ps can be clearly distinguished at the wavelength of 1050 nm. The details of the temporal intensity profile (Fig. 4(b)) are in clear agreement with the characteristic hyperbolic secant shape of a fundamental soliton as also reflected in the value of the soliton number *N* that has been estimated to 1.1. The associated trapped pulse in the normal dispersion regime temporally follows the soliton with a wavelength decreasing down to nearly 400 nm.

Note that solitons also appear in the vicinity of the pump. Indeed, XPM between the Stokes wave and the pump leads to modulation instability [1] and spectrally broadens the initial signal so that it can enter in the anomalous dispersion regime.

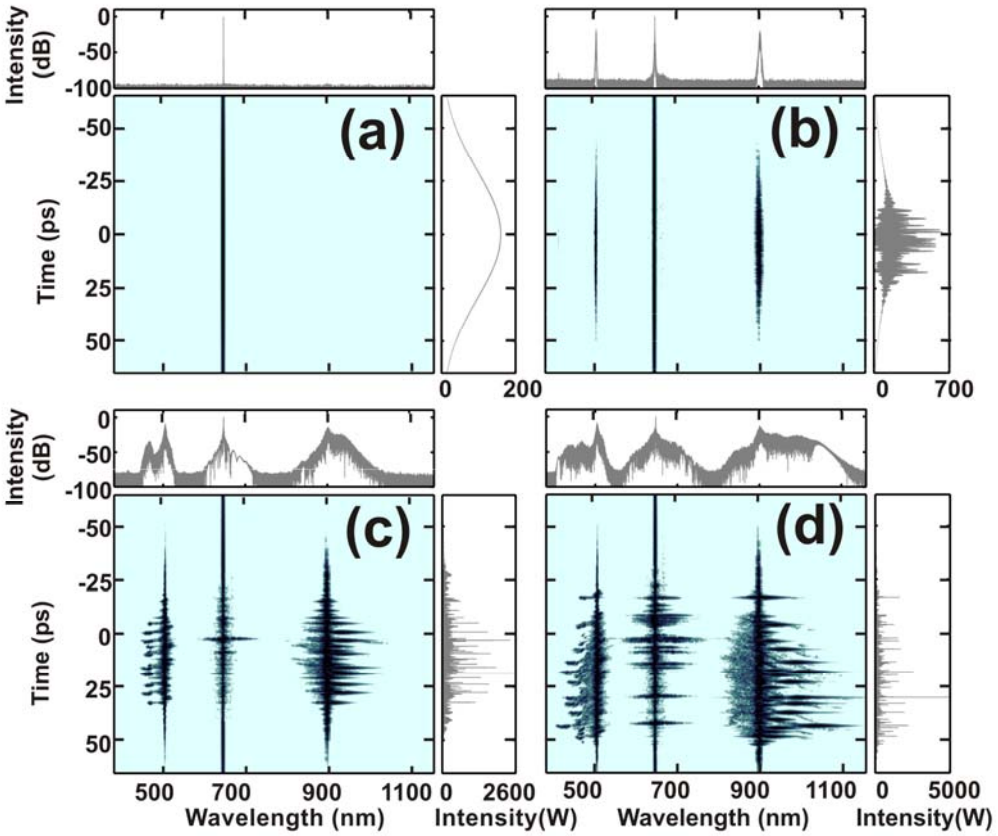

Fig. 3. Spectro-temporal representations of optical field for various propagation lengths : **(a)** 0 m, **(b)** 0.5 m, **(c)** 1.0 m et **(d)** 1.5 m.

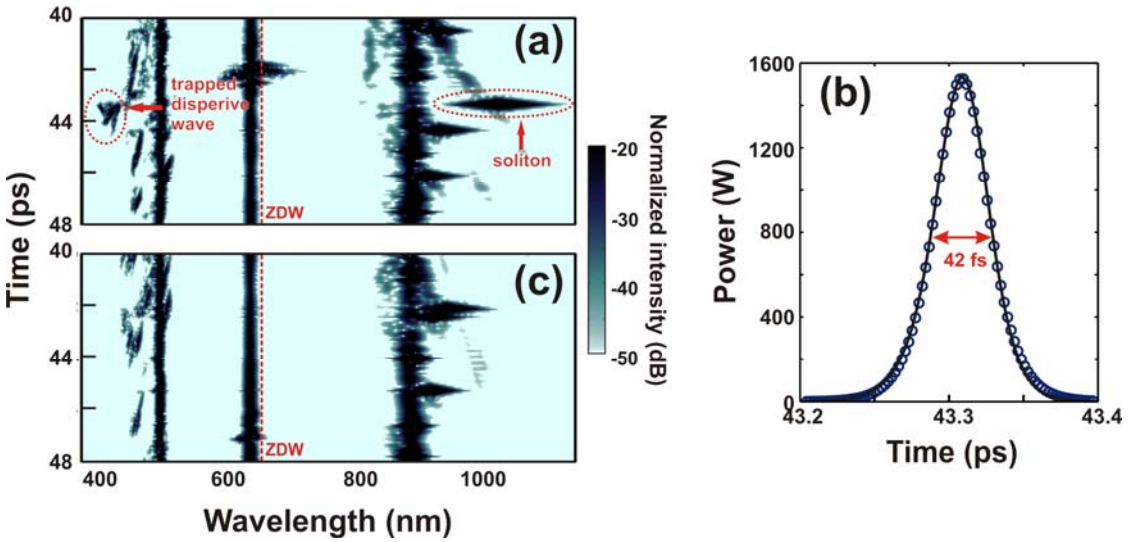

Fig. 4. (a) Magnification of Fig. 3(d) between 40 and 48 ps. (b) Temporal intensity profile of the most red-shifted optical structure. The result is compared with an hyperbolic secant fit (circles). (c) Spectro-temporal representation of another shot.

4. Statistical distributions

Spectrogram of Fig. 3 is based on a single numerical realization. However, as already suggested by the optical spectra of Fig. 1(c), the obtained results differ markedly from shot to shot, which can be further noticed from the details the spectrograms obtained for two shots (Fig. 4(a) and 4(c)). Consequently, one may wonder if extreme-values statistics similar to the ones that have been reported in usual modulation instability based supercontinua can be recorded. Indeed, it has recently been demonstrated that for an anomalous dispersion regime, the initial quantum noise can translate through scalar modulation instability into large intensity fluctuations [29-34]. In this important open area of research, some preliminary links have been suggested with the infamous and destructive hydrodynamic rogue waves [29, 32].

In order to measure the statistical distribution of the properties of the emerging optical structures, we have run 250 simulations in the presence of different random noise at a level corresponding to 1% shot-to-shot fluctuations in initial peak power. Among the tens of solitons that emerge in the Stokes wave, we have systematically recorded, for different distances of propagation, the peak-power of the most intense pulse. In order to isolate the Stokes wave and the associated solitons, we have numerically used a low-pass filter with a frequency edge at -75 THz. A similar analysis has been carried out for the trapped dispersive waves (with a high-pass optical filter having a frequency edge at +140 GHz). Note that, under XPM-induced modulation instability, the pump has also split into ultrashort structures and exhibits particularly apparent fluctuations (see Fig. 1(c) around 700 nm). Indeed, the pump spectral broadening occurring after 0.75 m allows the soliton generation across the zero dispersion wavelength, and several rare events are characterized by a significant soliton self-frequency shift in the anomalous dispersion regime.

Resulting probability distributions are summarized in Fig. 5. At 0.5 m (Fig. 5(a1)), peak powers are distributed nearly similarly around the median power, which corresponds to a close-to-Gaussian statistics. After 1 meter of propagation (Fig. 5(a2)), maximum peak power of the ultrashort pulses have increased by more than 10 dB, the distribution has significantly spread and a tail towards high-power appears. Saturation of the amplification process is visible at 1.5 m (Fig. 5(a3)). More interestingly, the tail develops so that the histogram exhibits the L-shape typical of extreme events [29] and several rare events present a peak power twice the median value.

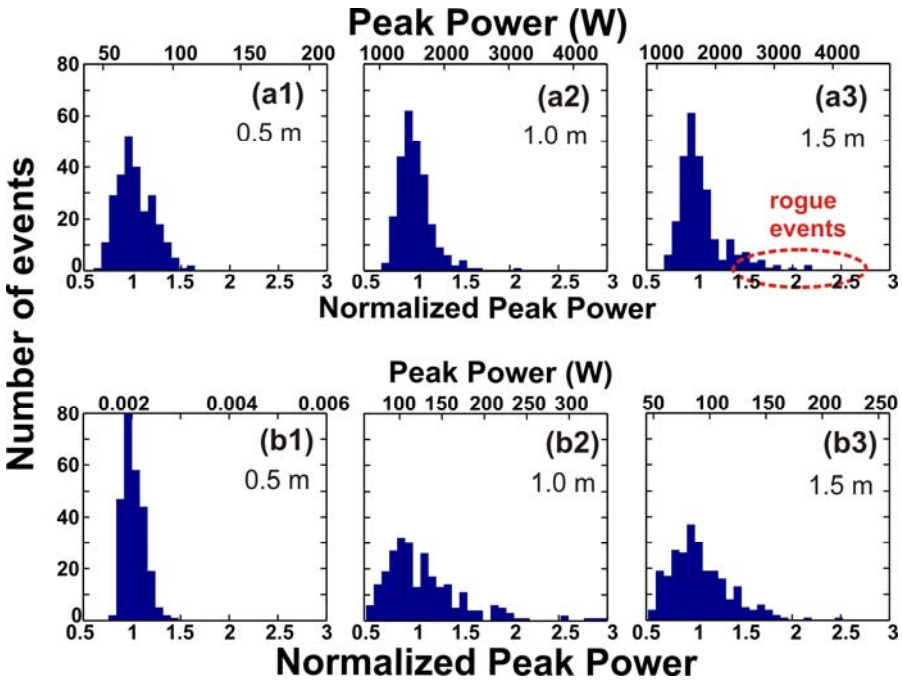

Fig. 5. Statistical distribution of the peak powers for the soliton pulses in the Stokes band **(a)** and dispersive trapped waves **(b)** for different lengths of propagation : **(1)** 0.5 m, **(2)** 1.0 m et **(3)** 1.5 m. Results are normalized relative to the median value (bottom) or expressed in Watts (top). 30 bins are used.

If solitons and trapped dispersive waves do not present exactly the same statistics, it is clear from Fig. 5(b) that their behaviors are intimately correlated, as recently suggested in [33]. Indeed, the trapping effect works out in such a way that solitons with higher power and subsequent larger frequency shift (corresponding to rogue events in the Stokes band) induce larger blue-shift of trapped dispersive waves. Let us however note that compared to [33], due to quasi-continuous nature of the pump, the situation of the present study clearly demonstrates that rogue events can be induced by fourth-order scalar MI and simultaneously appear in the spectral domain symmetrically and far from the initial pump wavelength. Moreover, another process that also occurs in our configuration of quasi-continuous initial pumping is the collision between various optical structures evolving at different velocities [32, 34].

5. Conclusion

In conclusion, we have carefully studied the process of wavelength conversion by fourth-order modulation instability. Our numerical results show an excellent agreement with experimental results previously published [6] and lead to several major conclusions. First, our study allows us to highlight the emergence of ultra-short fundamental solitons experiencing Raman self-frequency shift. This red-shift also induces a blue-shift of the anti-Stokes band indicating the presence of an optical radiation trapping by solitons which could be used to reach lower wavelengths. Moreover, a statistical analysis has revealed the emergence of rare but intense pulses that deviate strongly from the average behavior and from a Gaussian statistical distribution. In particular, after a given distance of propagation, the L-shape signature of rogue events has been shown for both Stokes and anti-Stokes pulses. Indeed, these results also demonstrate that optical rogue waves can be induced by directly pumping in the normal dispersion regime with a quasi-continuous wave, through a new window of modulation instability. This work outlines that the present system also allows the generation of optical rogue waves in a third spectral region near the pump wavelength in the vicinity of the zero dispersion wavelength.

All those points are therefore crucial for the design of compact, stable, reliable and cost-efficient fiber format components for ultra broadband wavelength conversion. In a wider context, it stresses once again the need of a careful research of potential extreme events that can emerge in optical amplifiers with instantaneous gain [35-37]. Furthermore, we believe our results provide some significant practical insights for an improved understanding of the initial formation of white-light supercontinua based on scalar 4^{th} order dispersion modulation instability [20, 21].

Acknowledgments

We would like to thank S. Pitois for illuminating discussions. This work was supported by the Agence Nationale de la Recherche (ANR MANUREVA project: ANR-08-SYSC-019) and by the Conseil Régional de Bourgogne.

References

[1] G. P. Agrawal, *Nonlinear Fiber Optics, Fourth Edition*. San Francisco, CA: Academic Press, 2006.

[2] K. Tai, A. Hasegawa, and A. Tomita, "Observation of modulational instability in optical fibers," *Phys. Rev. Lett.,* vol. 56, pp. 135-138, 1986.

[3] R. H. Stolen and J. E. Bjorkholm, "Parametric amplification and frequency conversion in optical fibers," *IEEE J. Quantum Electron.,* vol. 18, pp. 1062-1072, 1982.

[4] M. E. Marhic, N. Kagi, T.-K. Chiang, and L. G. Kazovsky, "Broadband fiber optical parametric amplifiers," *Opt. Lett.,* vol. 21, pp. 573-575, 1996.

[5] E. Seve, P. Tchofo-Dinda, G. Millot, M. Remoissenet, J. M. Bilbault, and M. Haelterman, "Modulational instability and critical regime in a highly birefringent fiber," *Phys. Rev. A,* vol. 54, pp. 3519-3533, 1996.

[6] G. Millot, S. Pitois, P. Tchofo-Dinda, and M. Haelterman, "Observation of modulational instability induced by velocity-matched cross-phase modulation in a normally dispersive bimodal fiber," *Opt. Lett.,* vol. 22, pp. 1686-1688, 1997.

[7] S. Pitois and G. Millot, "Experimental observation of a new modulational instability spectral window induced by fourth-order dispersion in a normally dispersive single-mode optical fiber," *Opt. Commun.,* vol. 226, pp. 415-422, 2003.

[8] J. D. Harvey, R. Leonhardt, S. Coen, G. K. L. Wong, J. C. Knight, W. J. Wadsworth, and J. S. Russell, "Scalar modulation instability in the normal dispersion regime by use of a photonic crystal fiber," *Opt. Lett.,* vol. 28, pp. 2225-2227, 2003.

[9] P. S. J. Russell, "Photonic-Crystal Fibers," *J. Lightw. Technol.,* vol. 24, pp. 4729-4749, 2006.

[10] L. Lavoute, W. J. Wadsworth, and J. C. Knight, "Efficient four wave mixing from a picosecond fibre laser in photonic crystal fibre," in *CLEO*, Munich, 2009, pp. paper cj5.4-thu.

[11] M. Szpulak and S. Février, "Chalcogenide As2S3 suspended core fiber for mid-IR wavelength conversion based on degenerate four-wave mixing," *IEEE Photon. Technol. Lett.,* 2009.

[12] V. Tombelaine, A. Labruyère, J. Kobelke, K. Schuster, V. Reichel, P. Leproux, V. Couderc, R. Jamier, and H. Bartelt, "Nonlinear photonic crystal fiber with a structured multi-component glass core for four-wave mixing and supercontinuum generation," *Opt. Express,* vol. 17, pp. 15392-15401, 2009.

[13] M. A. Foster, A. C. Turner, R. Salem, M. Lipson, and A. L. Gaeta, "Broad-band continuous-wave parametric wavelength conversion in silicon nanowaveguides," *Opt. Express,* vol. 15, pp. 12949-12958, 2007.

[14] G. K. L. Wong, A. Y. H. Chen, S. G. Murdoch, R. Leonhardt, J. D. Harvey, N. Y. Joly, J. C. Knight, W. J. Wadsworth, and P. S. J. Russell, "Continuous-wave tunable optical parametric generation in a photonic-crystal fiber," *J. Opt. Soc. Amer. B,* vol. 22, pp. 2505-2511, 2005.

[15] J. S. Y. Chen, S. G. Murdoch, R. Leonhardt, and J. D. Harvey, "Effects of dispersion fluctuations on widely tunable optical parametric amplification in photonic crystal fibers," *Opt. Express,* vol. 14, pp. 9491-9501, 2006.

[16] B. Kibler, C. Billet, J. M. Dudley, R. S. Windeler, and G. Millot, "Effects of structural irregularities on modulational instability phase matching in photonic crystal fibers," *Opt. Lett.,* vol. 29, pp. 1903-1905, 2004.

[17] J. M. Dudley, G. Genty, and S. Coen, "Supercontinuum generation in photonic crystal fiber," *Rev. Modern Physics,* vol. 78, pp. 1135-1184, 2006.

[18] B. Kibler, J. M. Dudley, and S. Coen, "Supercontinuum generation and nonlinear pulse propagation in photonic crystal fiber : influence of the frequency-dependent effective mode area," *Appl. Phys. B,* vol. 81, pp. 337-342, 2005.

[19] T. Sloanes, K. McEwan, B. Lowans, and L. Michaille, "Optimisation of high average power optical parametric generation using a photonic crystal fiber," *Opt. Express,* vol. 16, pp. 19724-91733, 2008.

[20] A. Kudlinski, V. Pureur, G. Bouwmans, and A. Mussot, "Experimental investigation of combined four-wave mixing and Raman effect in the normal dispersion regime of a photonic crystal fiber," *Opt. Lett.,* vol. 33, pp. 2488-2490, 2008.

[21] W. J. Wadsworth, N. Joly, J. C. Knight, T. A. Birks, F. Biancalana, and P. S. J. Russell, "Supercontinuum and four-wave mxing with Q-switched pulses in endlessly single-mode photonic crystal fibres," *Opt. Express,* vol. 12, pp. 299-309, 2004.

[22] F. M. Mitschke and L. F. Mollenauer, "Discovery of the soliton self-frequency shift," *Opt. Lett.,* vol. 11, pp. 659-661, 1986.

[23] E. Räikkönen, G. Genty, O. Kimmelma, M. Kaivola, K. P. Hansen, and S. C. Buchter, "Supercontinuum generation by nanosecond dual-wavelength pumping in microstructured optical fibers," *Opt. Express,* vol. 14, pp. 7914-7923, 2006.
[24] V. Tombelaine, P. Leproux, V. Couderc, and A. Barthelemy, "Visible supercontinuum generation in holey fibers by dual-wavelength subnanosecond pumping," *IEEE Photon. Technol. Lett.,* vol. 18, pp. 2466-2468, 2006.
[25] N. Nishizawa and T. Goto, "Pulse trapping by ultrashort soliton pulses in optical fibers across zero-dispersion wavelength," *Opt. Lett.,* vol. 27, pp. 152-154, 2002.
[26] A. V. Gorbach and D. V. Skryabin, "Light trapping in gravity-like potentials and expansion of supercontinuum spectra in photonic-crystal fibres," *Nature Photonics,* vol. 1, pp. 653-657, 2007.
[27] J. C. Travers, "Blue solitary waves from infrared continuous wave pumping of optical fibers," *Opt. Express,* vol. 17, pp. 1502-1507, 2009.
[28] A. Kudlinski, G. Bouwmans, M. Douay, M. Taki, and A. Mussot, "Dispersion-engineered photonic crystal fibers for CW-pumped supercontinuum sources," *J. Lightw. Technol.,* vol. 27, pp. 1556-1564, 2009.
[29] D. R. Solli, C. Ropers, P. Koonath, and B. Jalali, "Optical rogue waves," *Nature,* vol. 450, p. 1054, 2007.
[30] J. M. Dudley, G. Genty, and B. J. Eggleton, "Harnessing and control of optical rogue waves in supercontinuum generation " *Opt. Express,* vol. 16, pp. 3644-3651, 2008.
[31] B. Kibler, C. Finot, and J. M. Dudley, "Soliton and rogue wave statistics in supercontinuum generation in photonic crystal fibre with two zero dispersion wavelengths," *Eur. Phys. J. Special Topics,* vol. 173, pp. 273-279, 2009.
[32] A. Mussot, A. Kudlinski, M. I. Kolobov, E. Louvergneaux, and M. Taki, "Convective instabilities and optical rogue waves in fibers with CW pumping," in *LEOS Winter Topical Meeting*, Innsbruck, 2009, p. TUC2.5.
[33] M. Erkintalo, G. Genty, and J. M. Dudley, "Rogue wave like characteristics in femtosecond supercontinuum generation," *Opt. Lett.,* vol. 34, pp. 2468-2470, 2009.
[34] G. Genty, J. M. Dudley, and B. J. Eggleton, "Modulation control and spectral shaping of optical fiber supercontinuum generation in the picosecond regime," *Appl. Phys. B,* 2008.
[35] K. Hammani, C. Finot, J. M. Dudley, and G. Millot, "Optical rogue-wave fluctuations in fiber Raman amplifiers," *Opt. Express,* vol. 16, pp. 16467-16474, 2008.
[36] K. Hammani, C. Finot, and G. Millot, "Emergence of extreme events in fiber-based parametric processes driven by a partially incoherent wave," *Opt. Lett.,* vol. 34, pp. 1138-1140, 2009.
[37] D. Borlaug, S. Fathpour, and B. Jalali, "Extreme value statistics in silicon photonics," *IEEE Photon. J.,* vol. 1, pp. 33-39, 2008.